AD-A049 188 ARIZONA UNIV TUCSON DEPT OF AEROSPACE AND MECHANICA--ETC F/G 20/4
UNSTEADY TRANSONIC FLOW COMPUTATIONS,(U)
SEP 77 A R SEEBASS, N J YU, K FUNG N00014-76-C-0182
NL

UNCLASSIFIED

1 OF 1
AD
A049188

END
DATE
FILMED
3-78
DDC

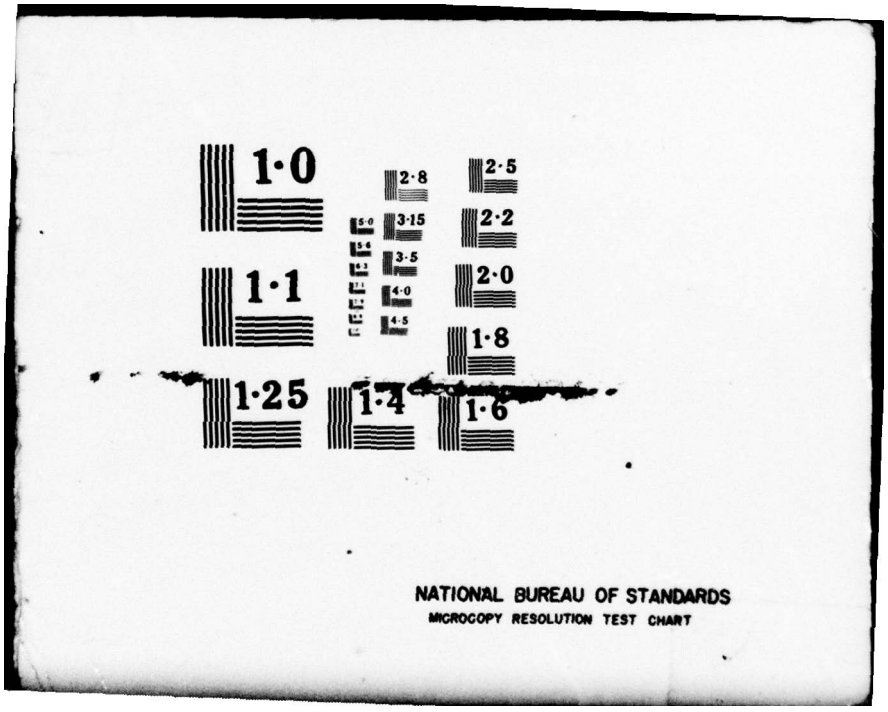
1·0
1·1
1·25
1·4
1·6
1·8
2·0
2·2
2·5
2·8
3·15
3·5
4·0
4·5
5·0
NATIONAL BUREAU OF STANDARDS
MICROCOPY RESOLUTION TEST CHART

UNCLASSIFIED
SECURITY CLASSIFICATION OF THIS PAGE (When Data Entered)

12

REPORT DOCUMENTATION PAGE	READ INSTRUCTIONS BEFORE COMPLETING FORM
1. REPORT NUMBER	2. GOVT ACCESSION NO. 3. RECIPIENT'S CATALOG NUMBER
4. TITLE (and Subtitle) (6) UNSTEADY TRANSONIC FLOW COMPUTATIONS,	5. TYPE OF REPORT & PERIOD COVERED 6. PERFORMING ORG. REPORT NUMBER
7. AUTHOR(s) (10) A. R. Seebass, N. J. Yu K-Y. Fung	8. CONTRACT OR GRANT NUMBER(s) (15) N00014-76-C-0182, AFOSR-76-2954B
9. PERFORMING ORGANIZATION NAME AND ADDRESS University of Arizona Aerospace and Mechanical Engineering Tucson, Arizona 85721	10. PROGRAM ELEMENT, PROJECT, TASK AREA & WORK UNIT NUMBERS NR 061-231
11. CONTROLLING OFFICE NAME AND ADDRESS Office of Naval Research (Code 438) Arlington, Virginia 22217	12. REPORT DATE (11) Sep[redacted]77 13. NUMBER OF PAGES 17
14. MONITORING AGENCY NAME & ADDRESS (if different from Controlling Office) ONR Resident Representative Room 421-Space Science Building University of Arizona Tucson, Arizona 85721 (12) 35 p.	15. SECURITY CLASS. (of this report) UNCLASSIFIED 15a. DECLASSIFICATION/DOWNGRADING SCHEDULE

16. DISTRIBUTION STATEMENT (of this Report)

Approved for Public Release; distribution unlimited.

17. DISTRIBUTION STATEMENT (of the abstract entered in Block 20, if different from Report)

18. SUPPLEMENTARY NOTES

19. KEY WORDS (Continue on reverse side if necessary and identify by block number)

Transonic flow
Unsteady flow

20. ABSTRACT (Continue on reverse side if necessary and identify by block number)

The effects of unsteady modes of motion on two-dimensional transonic flows are investigated. Numerical algorithms that treat shock waves as moving discontinuities are described for nonlinear and time-linearized perturbation flows. Results for transonic flow past an NACA 64A006 airfoil experiencing harmonic motions in one of several modes are presented.

DD FORM 1 JAN 73 1473 EDITION OF 1 NOV 65 IS OBSOLETE
S/N 0102-LF-014-6601

UNCLASSIFIED 402 192
SECURITY CLASSIFICATION OF THIS PAGE (When Data Entered)

UNSTEADY TRANSONIC FLOW COMPUTATIONS

by

A. R. Seebass, N. J. Yu, K-Y. Fung

Department of Aerospace and Mechanical Engineering
University of Arizona, Tucson, Arizona 85721

Presented at the

AGARD Fluid Dynamic Panel Symposium on

UNSTEADY AERODYNAMICS

Ottawa, Canada, September 26-28, 1977

This research was sponsored by the AFOSR through Grant 76-2954B, the NASA through Grant 2112, and the ONR through Contract N0014-76-C-0182.

UNSTEADY TRANSONIC FLOW COMPUTATIONS

by

A. R. Seebass, N. J. Yu, and K-Y. Fung

Department of Aerospace and Mechanical Engineering
University of Arizona
Tucson, Arizona 85721

SUMMARY

We investigate the effects of unsteady modes of motion on two-dimensional transonic flows; wo do so in the context of the inviscid small perturbation approximation. The study is a numerical one and draws upon the alternating-direction implicit procedure developed for such calculations by Ballhaus and his coworkers at the NASA Ames Research Center. Our numerical algorithm treats shock waves as moving discontinuities. Results of nonlinear and time-linearized calculations of the transonic flow past an NACA 64A006 airfoil experiencing harmonic motions in several of its modes are presented and discussed.

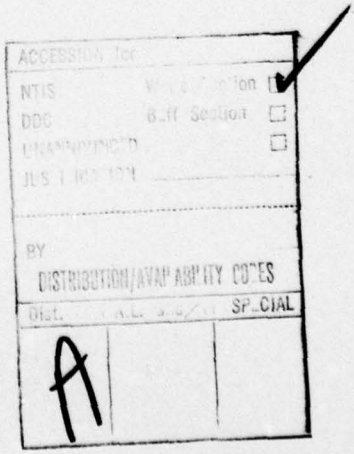

1. INTRODUCTION

In unsteady transonic flows, relatively small periodic changes in the boundary conditions can lead to substantial changes in the loads and moments with marked phase lags. These are of major concern in the aerodynamic design of aircraft that operate in the transonic regime. A short, but timely, review of various aspects of unsteady transonic flow may be found in Reference 1. Of particular concern are aero-elastic behavior, and flutter and buffet boundaries. Here the unsteady perturbations may sometimes be small enough that linearization about a nonlinear steady flow, as suggested by Landahl (2) long ago, is possible.

In such flows the behavior of the boundary layer, especially as it is affected by the pressure rise caused by any shock waves in the flow, is clearly of major importance. Additionally, in the neighborhood of the leading edge the flow perturbations are large; consequently, highly accurate inviscid results require the use of the full potential equation. It seems likely that eventually the computational algorithms used in routine studies of unsteady transonic flows will use the Reynolds averaged Navier-Stokes equations now used in research studies. However, such algorithms (3) currently require substantial computer time and are too inefficient for exploratory studies such as this one. The ability of these algorithms to model complex unsteady transonic flow phenomena, such as buffet, has recently been demonstrated (4).

An important consideration in constructing an algorithm for unsteady transonic flows is the treatment of moving shock waves. The experimental observations of Tijdeman (5-7) indicate that even for simple airfoil motions shock wave motions can be complicated, and that they can strongly affect aerodynamic force and moment variations. Time-linearized methods, i.e.,

methods that assume the unsteady perturbations are small compared to the basic steady disturbance, have not usually considered shock motions (8, 9), although they can be modified to do so for small shock excursions (10). Time-integration methods (11-18) treat shock waves by "capturing" them, a procedure that can present a number of difficulties.

Unsteady experiments (5-7), analysis (10) and numerical studies (10) all indicate that the amplitude of the shock wave motions increases inversely with reduced frequency. Thus some of the most important effects occur with low-frequency motions. This is not surprising; nonlinear behavior is suppressed at higher frequencies, with the small perturbation equation becoming linear for frequencies higher than the two-thirds power of the airfoil's thickness-to-chord ratio. Explicit finite-difference schemes are not efficient when applied to low-frequency cases because the stability restriction on the time step is substantially more severe than that required for accuracy. As a result, efficient semi-implicit methods (13) and even more efficient fully implicit methods (11, 12, 17, 18) have been developed. Caradonna and Isom (17) use an iterative implicit procedure, i.e., the nonlinear implicit finite-difference equations must be solved iteratively at a given time level. In an earlier, unpublished, study we also used such a procedure. Ballhaus and Steger (11) and Beam and Warming (18) constructed more efficient algorithms that solve the nonlinear equations directly by the solution of simple matrix equations generated by an alternating-direction implicit (ADI) procedure. This method has proven to be so efficient that it is now used as an alternative to successive line over-relaxation (SLOR) for steady flow calculations (Reference 19 and Yu and Seebass, unpublished).

As mentioned above, these implicit schemes "capture" shock waves, i.e., shock waves evolve automatically as part of the numerical solution. Shock

capturing produces shock profiles that are distorted in a manner than depends on the truncation errors in the finite-difference scheme. The use of mixed-difference schemes (11, 18) can improve the situation for cases in which the flow changes from supersonic to subsonic across the shock. However, when this condition is not satisfied the differencing cannot be switched across the shock and shock resolution is poor. In any case, shock capturing requires spatial grid spacings, in regions where shock waves are anticipated, that are sufficiently small to resolve the shock waves. The grid spacing required to do this is usually much smaller than that required to resolve flow variable gradients in most of the rest of the flow field. Shock fitting removes the large gradients from the finite difference solution and permits equivalent flow field resolution with fewer grid points, both in space and time (20, 21). If shock waves are not treated as discontinuities, but are to be captured correctly, the difference equations must be solved in conservation form. This imposes an additional constraint on the construction of finite-difference schemes that can be difficult to satisfy.

A need for shock fitting also arises in computing time-linearized solutions for very small unsteady perturbations. Time-linearized solutions for indicial motions can be used to determine force and moment coefficient variations at various reduced frequencies, obviating the need for a numerical solution at each reduced frequency (see, e.g., Reference 22).

Traci, et al., (8, 23, 24) have developed relaxation methods for solving the resulting time-linearized equations of motion for harmonic disturbances. Less complete, but comparable, studies have been made by Weatherill et al. (9); these derive from an earlier study by Ehlers (25). In both of these studies shock motions, which contribute substantially to the time-varying loads and moments, are neglected. Difficulties also arise in the convergence

of the iterative numerical scheme. Unsteady small amplitude motions have shock wave excursions that are the order of the amplitude of the motion divided by the reduced frequency of the motion. Consequently, these shock motions dominate other low frequency contributions to the lift and moment coefficients. Such time-linearized shock motions can be computed in a rational way, but the accuracy of the results depends critically on an accurate resolution of the steady flow field in the vicinity of the shock wave (10); this is best accomplished by shock fitting.

This paper briefly reviews the numerical procedures we have developed for computing nonlinear and time-linearized small perturbation unsteady transonic flows. We use an ADI scheme and treat shock waves as discontinuities in the flow. Calculations of the transonic flow past an NACA 64A006 airfoil experiencing harmonic or indicial pitching and flap oscillations are discussed.

2. FORMULATION

We write the unsteady small disturbance equation for low frequency transonic flows in the commonly used form

$$-2KM_\infty^2\phi_{xt} + \{1 - M_\infty^2 - (\gamma + 1)M_\infty^2\phi_x\}\phi_{xx} + \phi_{yy} = 0. \qquad (1)$$

The spatial coordinates, the time, and the velocity potential in (1) have been non-dimensionalized by the chord, the reciprocal of the angular frequency, and the free stream velocity times the chord, respectively. Other, perhaps more useful and suitable, forms are given in References 21 and 26. This equation results from a systematic expansion of the velocity potential in the thickness ratio τ and applies for reduced frequencies $K = O(\tau^{2/3})$

where $K = \omega c/U$, i.e., the angular frequency multiplied by the time it takes the flow to traverse the airfoil chord. Lin, Reisner and Tsien (27) showed that, with restriction to small perturbations throughout the flow, this is the only nonlinear equation that arises. For moderate frequencies the equation

$$-K^2\phi_{tt} - 2K\phi_{xt} + \{1 - M_\infty^2 - (\gamma + 1)M_\infty^2[\phi_x + \frac{\gamma - 1}{\gamma + 1} K\phi_t]\}\phi_{xx} + \phi_{yy} = 0$$

is frequently used, with or without the ϕ_t term, and may provide results that apply at higher frequencies than those obtained from (1).

The boundary condition on the body takes the simple form

$$\phi_y(x,0,t) = \tau[Y^\circ_x + \frac{\delta}{\tau} (Y^u_x + KY^u_t)], \quad -\frac{1}{2} \leq x \leq \frac{1}{2}, \tag{2}$$

where $Y(x,t)$, the instantaneous body shape, has been decomposed into a steady part, Y°, and an unsteady part, Y^u. Here δ is the amplitude of the unsteady oscillation. Because $K = 0(\tau^{2/3})$, the last term in (2) is dropped unless $Y^u_x \equiv 0$ or is small. For this reason, the time-linearized perturbation velocity potential for plunging motions $(Y^u_x = 0)$ is just K times that for the analogous pitching motion, where $Y^u(x,t) = (x - x_o)\sin t$.

Numerical studies conducted by Magnus (15) show that erroneous boundary data on a finite domain can lead to significant errors. The low frequency approximation implies that any changes in the circulation are communicated instantly downstream to infinity. Consequently, the simplest boundary conditions are $\phi_x = 0$ on the downstream boundary and $\phi = 0$ on the other boundaries. Ballhaus and Goorjian (12) used these boundary conditions in their study and obtained satisfactory results. The validity of such far-

field boundary conditions can only be justified by numerical experiments; i.e., near the boundary the disturbance quantities ϕ_x, and ϕ_y, must be much smaller than the values at the airfoil surfaces. For the lifting case, ϕ depends on the instantaneous circulation, Γ. This dependence can be derived theoretically by assuming that in the far field all the perturbations are small compared to the basic steady state (see, e.g., Reference 26). Here we use a stretched coordinate system that maps the doubly infinite domain into $|\xi| \leq 1$, $|\eta| \leq 1$, and set $\phi_x = 0$ on the downstream boundary $\xi = 1$ and $\phi = 0$ elsewhere on the boundary of this domain. As a numerical test for this procedure we have computed the steady state circulation about an NACA 64A006 airfoil for various flap deflection angles, using the ADI method with appropriate far-field values of ϕ, corrected for the usual steady state circulation contribution. These results have been compared with the results obtained by the ADI calculations with the boundary conditions employed here for an unsteady flap deflection to the correct angle. These results are identical within the accuracy with which we have computed the solutions.

Any shock wave that exists in the flow field must satisfy the jump relation derived from the conservative form of the governing equation (1), namely

$$-2KM_\infty^2[\phi_x]^2(dx/dt)_s - \{1 - M_\infty^2 - (\gamma + 1)M_\infty^2\tilde{\phi}_x\}[\phi_x]^2 + [\phi_y]^2 = 0 \qquad (3)$$

together with the condition derived from the assumption of irrotationality,

$$(dy/dx)_s = -[\phi_x]/[\phi_y]. \qquad (4)$$

Here $\tilde{\phi}_x$ refers to the mean value of ϕ_x evaluated on each side of the discontinuity, and $[\phi_x]$ indicates the jump in ϕ_x across the discontinuity; the subscript "s" denotes the quantity evaluated at the shock surface.

The pressure coefficient, defined so that it vanishes at sonic conditions, takes the form

$$C_p = -2 \left\{ \frac{M_\infty^2 - 1}{(\gamma + 1)M_\infty^2} + \phi_x \right\} . \tag{5}$$

In the small disturbance approximation, the Kutta condition is imposed by requiring that C_p be continuous at $y = 0$ for $x > 1/2$.

2.1 Time-Linearized Equations

We now assume that the unsteady disturbances, characterized by δ, are small enough that we may write

$$\phi(x,y,t) = \phi^\circ(x,y) + \delta\psi(x,y,t) + o(\delta) \tag{6}$$

and neglect higher-order terms in δ. The restriction imposed on δ for this to be true will depend on the other parameters of the problem, viz., $\kappa \equiv (1 - M_\infty^2)/[(\gamma + 1)M_\infty^2\tau]^{2/3}$ and K. This gives

$$\{1 - M_\infty^2 - (\gamma + 1)M_\infty^2\phi_x^\circ\}\phi_{xx}^\circ + \phi_{yy}^\circ = 0, \quad \phi_y^\circ(x,0) = \tau Y^{\circ\prime}(x), \quad -\tfrac{1}{2} \le x \le \tfrac{1}{2} ; \tag{7}$$

$$-2KM_\infty^2\psi_{xt} + \{[1 - M_\infty^2 - (\gamma + 1)M_\infty^2\phi_x^\circ]\psi_x\}_x + \psi_{yy} = 0,$$

$$\psi_y(x,0,t) = Y_x^u + KY_t^u, \quad -\tfrac{1}{2} \le x \le \tfrac{1}{2} . \tag{8}$$

The solution to (7) must satisfy the steady version of the shock relations (4) and (5). The shock relations for (8) are discussed in Section 2.2.

We avoid writing

$$\psi(x,y,t) = \mathrm{Re}\{\bar{\psi}(x,y)e^{i\omega t}\} \tag{9}$$

as this restricts the study to harmonic motions. Because indicial motions can be superimposed to obtain the results for any frequency, they seem more important. Equation (9) results in an equation for a complex-valued $\bar{\psi}$ which may be solved by line relaxation. Our experience with unsteady ADI techniques has been that they are at least as effective as line relaxation for problems of this type, and hence there is no advantage to the decomposition (9).

The numerical algorithm developed in Reference 21 and described briefly in Section 3 can be used to solve the basic equation (1) subject to the boundary conditions (2), the shock conditions, (3) and (4), the far-field boundary conditions and the Kutta condition. Steady state solutions, $\phi^{\circ}(x,y)$, may be obtained rapidly by subjecting a basic steady state, such as undisturbed flow, to rapidly changing boundary data until a new steady configuration is prescribed. This, then, determines the steady state result for (7) needed to solve (8).

2.2 Shock Fitting

The basic algorithm for shock fitting in mixed flows was developed in a previous study of steady transonic flows (20). A different approach to shock fitting has also been used by Hafez and Cheng (28) in their study of steady transonic flow problems. Their procedure essentially replaced the shock-point operator of Murman (29) by an analogous difference statement derived from the shock jump conditions. Subsequently, the velocity potential on each side of the shock wave is extrapolated to locate the shock wave.

To understand the shock-fitting procedure for unsteady transonic flow calculations it is necessary to recall how shock waves form in an unsteady field. Shock waves are generated when the local flow becomes supersonic and compressive. While the initial shock formation may not be predicted exactly by the numerical solution when shock fitting is used in the early stages of shock wave formation, it eliminates spurious oscillations in the numerical solution and does provide the correct development of the shock wave in later stages of the calculations (30). The criteria that we set for the initial shock formation is that the local flow become sonic (relative to the airfoil) and compressive. In the body-fixed coordinate system, a shock wave can exist both in the usual supersonic-supersonic and supersonic-subsonic transitions, but also in a purely subsonic flow field, sometimes referred to as a "subsonic-subsonic" shock. In any case, the flow ahead of the shock relative to a coordinate system fixed on the shock must be always supersonic. Consequently, the correct judgment for the existence of a shock wave in the unsteady field is to evaluate the local flow velocity ahead of a prospective shock with respect to the coordinate system fixed on it; i.e., if the local flow is supersonic a shock may exist, if the local flow becomes sonic the shock strength diminishes, and if it is subsonic a shock cannot exist.

Any shock wave that exists in the flow field must satisfy the jump relations (3) and (4). In two-dimensional small perturbation transonic flows the shock waves that usually occur are nearly normal to the flow direction. While it is not necessary to do so, in the numerical calculations reported here we have assumed that if the basic steady flow has a shock wave, then this shock may be approximated by a shock wave normal to the free stream flow. To be consistent with this approximation we must also assume that the motion of

any shock wave that arises from unsteady changes in the flow, as well as the motion of existing shock waves, is also calculated by this normal shock approximation. For this simplified model, (3) and (4) reduce to

$$[\![\phi]\!] = 0 \quad \text{on} \quad \dot{x}_s \equiv (dx/dt)_s = \frac{\gamma + 1}{2K} \left\{ \frac{M_\infty^2 - 1}{(\gamma + 1)M_\infty^2} + \tilde{\phi}_x \right\} , \tag{10}$$

which gives the speed of the normal shock in the flow field. For steady flows $\tilde{\phi}_x$ is a function of x alone; this, of course, still permits $[\![\phi_x]\!]$ to vary with y. For unsteady flows, while $\dot{x}_s$ is a function of t alone, the strength of the shock will still vary with y.

For time-linearized flows the steady state result for ϕ_x° with normal shock fitting will give a steady state shock position x_s°, $0 \leq |y| \leq y_\pm^*$. We now determine the shock wave's motion by writing the perturbed shock position as $x_s = x_s^\circ + \delta\chi(t)$ and using the time-linearized version of (10); we note that an expression of the form $x_s^\circ + \delta\chi(t)/K$ would probably be more appropriate. From (10), we conclude that the shock motion is governed by

$$\frac{d\chi}{dt} = \frac{\gamma + 1}{2K} \tilde{\psi}_x(x,0,t) \quad \text{with} \quad [\![\phi]\!] = [\![\phi^\circ]\!] + \delta[\![\psi]\!] = 0 \tag{11}$$

on the shock. Linearizing the expression in (11) for the velocity potential about the steady shock position we find

$$\phi(x_s,y,t) = \phi(x_s^\circ,y,t) + \phi_x(x_s^\circ,y,t)\delta d\chi$$

$$= \phi^\circ(x_s^\circ,y) + \phi_x^\circ(x_s^\circ,y)\delta d\chi + \delta\psi(x_s^\circ,y,t) + O(\delta^2).$$

Because we have treated the shock as a normal one, y appears here simply as a parameter. Now $[\![\phi(x_s,y,t)]\!]$ and $[\![\phi^\circ(x_s^\circ,y)]\!]$ are both zero; consequently

we have

$$[\![\psi(x_s^\circ,y,t)]\!] = -\frac{(\gamma+1)}{2K}[\![\phi_x^\circ(x_s^\circ,y)]\!]\int_0^{t} \psi_x(x_s^\circ,0,\hat{t})d\hat{t} \tag{12}$$

which must be integrated in time in conjunction with the solution to (8).

3. NUMERICAL PROCEDURES

In a preliminary study of the unsteady transonic flows a normal shock-fitting procedure was implemented in an implicit-iterative scheme. Satisfactory results were obtained, but the procedure was time-consuming because of the iterative process required at each time step. The recent studies of Ballhaus and Steger (11) and Ballhaus and Goorjian (22) show that an ADI scheme is more efficient than the implicit-iterative scheme in treating the low frequency transonic flows. The shock-fitting algorithm was modified and implemented with an ADI scheme. In this section the ADI procedure and the method used for unsteady shock fitting are briefly reviewed.

3.1 Coordinate Stretching

To minimize the far-field boundary effects on the numerical results a relatively large computational region is usually required. For some of the cases studied in this paper the shock excursions are large and the unsteady disturbances carried several chord lengths away from the airfoil; thus, the use of a relatively large computational domain seems desirable. A simple and straightforward way of computing the solution in a large computational domain is to use nonuniform mesh distributions with most of the mesh points concentrated in the region of interest. An alternative is to introduce analytical coordinate stretchings. In the present study, we use the following coordinate stretchings:

$$\xi = \pm\{1 - \exp(\mp a_1 x)\} \quad \text{for} \quad x \gtrless 0 \quad \text{and} \quad \eta = \pm\{1 - \exp(\mp a_2 y)\} \quad \text{for} \quad y \gtrless 0,$$

where a_1 and a_2 are constants that control the mesh distributions. The infinite physical domain is transformed into the finite computational domain bounded by $|\xi| \leq 1$, and $|\eta| \leq 1$. The transformation provides a concentrated mesh distribution near the airfoil which is suitable for the present study. While this scaling is not consistent with the known algebraic decay of the perturbations, calculations made with an algebraic scaling, viz., $\xi = x/(|x| + a_1)$ etc., gave essentially identical results. The exponential variation used here seems more desirable near the airfoil.

The governing equation (1), written in the stretched coordinate system, is

$$\left\{ \frac{-2KM_\infty^2}{a_2^2(1 - |\eta|)} \phi_\xi \right\}_t - \left\{ \frac{(\gamma + 1)M_\infty^2}{2a_2^2(1 - |\eta|)} \left[\frac{M_\infty^2 - 1}{(\gamma + 1)M_\infty^2} + a_1(1 - |\xi|)\phi_\xi \right]^2 \right\}_\xi$$

$$+ \left\{ \frac{1 - |\eta|}{a_1(1 - |\xi|)} \phi_\eta \right\}_\eta = 0. \tag{13}$$

Because (13) is in divergence-free form, a conservative difference approximation can be constructed if the shock wave is to be "captured" rather than "fitted."

The normal shock jump relation follows directly from (13); this relation and the boundary condition on the airfoil surface are now

$$(d\xi/dt)_s = \frac{a_1(1 - |\xi|)(\gamma + 1)}{2K} \left\{ \frac{M_\infty^2 - 1}{(\gamma + 1)M_\infty^2} + a_1(1 - |\xi|)\tilde{\phi}_\xi \right\} \tag{14}$$

and

$$\phi_\eta(0,\xi) = \frac{a_1}{a_2}\,(1 - |\xi|)\,\frac{\partial Y(\xi,t)}{\partial \xi} + \frac{K}{a_2}\,\frac{\partial Y(\xi,t)}{\partial t}\,,$$

$$-1 + \exp(a_1/2) \le \xi \le 1 - \exp(-a_1/2).$$

Equations analogous to (13) and (14) for the time-linearized results are given in Reference 10.

3.2 Alternating-Direction Implicit (ADI) Method

The low frequency equation in the stretched coordinate system is solved by the alternating-direction implicit scheme developed by Ballhaus and Steger (11). To simplify this discussion, equation (13) is rewritten in the form

$$\Psi_{\xi t} + F_\xi + G_\eta = 0, \tag{15}$$

where the function Ψ, F and G may be determined by comparing equations (13) and (15). The solution is advanced from time level "n" to level "n+1" by the following two-step procedure:

$$\frac{1}{\Delta t}\,(\Psi_\xi^+ - \Psi_\xi^n) + D_\xi F^+ + \delta_\eta G^n = 0; \quad \frac{1}{\Delta t}\,(\Psi_\xi^{n+1} - \Psi_\xi^+) + \frac{1}{2}\,\delta_\eta (G^{n+1} - G^n) = 0. \tag{16}$$

Here "+" refers to an intermediate value of Ψ, D_ξ is the type-dependent difference operator for ξ-derivatives and δ_η the central-difference approximation for η-derivative. The backward difference approximation for Ψ_ξ can be either a first-order or a second-order difference approximation, with the latter giving improved results. The nonlinear term F is evaluated, using a linearization somewhat different from the two-time level averaging procedure

of Ballhaus and Steger. The difference approximations described above provide first- or second-order accuracy for $\Psi_{\xi t}$, second-order accuracy for F_ξ and G_η in subsonic regions, and first-order accuracy for F_ξ in supersonic regions. A local analysis shows that the procedure is unconditionally stable.

In the first step a quadradiagonal system is generated and can be easily solved by direct elimination. For lifting calculations two grid lines are used to represent the lower and upper surfaces of the airfoil. The circulation, Γ, is calculated by $\Gamma = \phi^U_{ITE} - \phi^L_{ITE}$ through each sweep. Here "ITE" denotes the upper and lower values at the first grid point behind the trailing edge. This circulation is incorporated into the construction of the η-derivatives behind the airfoil for $\eta = 0$,

In the second step a tridiagonal system is generated by the body. Ahead of the leading edge and behind the trailing edge the double grid notation for $\eta = 0$ destroys the tridiagonal system. However, ahead of the leading edge, $\phi^U = \phi^L$, and behind the trailing edge, $\phi^U = \phi^L + \Gamma$; thus the difference equations can be reordered to give a tridiagonal system. On the airfoil surface, the matrix equations above and below the airfoil are decoupled; they can either be solved separately or simultaneously by packing the matrix equations together.

Again, analogous but somewhat simpler equations and procedures are used for the time-linearized calculations. In these calculations the type dependent operator, D_ξ, changes at the steady state sonic line and shock wave. The coefficient, $f(\xi,\eta)$, that appears in (8) in the form $\{f(\xi,\eta)\psi_\xi\}_\xi$ depends on the steady state results $\phi^\circ(\xi,\eta)$ and must be stored. On the other hand, the matrices used do not depend on the solution ψ and, consequently, need only be inverted once. In its present form our algorithm does not take advantage of this feature.

3.3 Shock Fitting

We start the unsteady nonlinear flow calculations by using an ADI scheme. When the local flow becomes sonic and compressive, we introduce the shock-fitting algorithm described in detail in Reference 21. Sonic, compressive points are treated as shock points where differentiation in t and ξ across discontinuities is avoided. Initially, the shock has zero strength and is stationary. The flow properties ahead of and behind the shock can be easily extrapolated from neighboring points. The shock wave can either increase or decrease in strength during the unsteady process. This results in three possibilities for shock motion that have to be considered separately in the fitting procedure: The shock moves upstream and crosses grid points; the shock remains stationary or moves within a grid spacing; the shock moves downstream and crosses grid points. At each new time level the shock position is determined by applying (10). The formulations of the difference approximations for each case are quite similar.

For time-linearized calculations the solution is advanced in time using the time-linearized analogues of (16) coupled with (12) in the form

$$[\![\psi]\!]^{+} = -C(\eta)\Delta t\tilde{\psi}_{\xi}^{n} + [\![\psi]\!]^{n}; \quad [\![\psi]\!]^{n+1} = -C(\eta)\Delta t\tilde{\psi}_{\xi}^{n+1} + [\![\psi]\!]^{+}.$$

Here

$$C(\eta) = \frac{\gamma + 1}{4K} a_1^2 (1 - |\xi_s^\circ|)^2 [\![\phi_\xi^\circ(\xi_s^\circ, \eta)]\!],$$

and ξ_s° denotes the steady state position of the shock wave. This procedure corrects the ψ values for shock motions as the solution progresses. The shock motion is easily determined simultaneously by using (11) and (12) in the form

$$\chi^{n+1}(0,t) = -[\![\psi(x_s^\circ,0,t)]\!]^{n+1}/[\![\phi_x(x_s^\circ,0)]\!].$$

Further details are given in Reference 10.

4. RESULTS AND DISCUSSION

Both the nonlinear and time-linearized algorithms have been used to compute the flow past an NACA 64A006 airfoil subjected to indicial, i.e., step, changes and harmonic motions in pitch and flap oscillation. The latter calculations have included a range of Mach numbers, amplitudes for the nonlinear algorithm, and reduced frequencies for the harmonic changes. The nonlinear algorithm has also been used to compute the flow past a pulsating parabolic arc airfoil. In this latter flow, at $M_\infty = 0.85$, as the airfoil thickens a shock wave forms and moves downstream until shortly after mid-cycle. As the airfoil thins, the shock wave moves upstream with increasing speed, eventually leaving the airfoil. A comparison of the results, with and without shock fitting (21), indicates that shock fitting predicts the formation of the shock wave more accurately. It also properly defines the shock wave when it becomes "subsonic-subsonic" in the fixed grid system. The shock wave decays slowly as it propagates into the free stream after passing the location of the leading edge when the airfoil's thickness has just become zero.

4.1 NACA 64A006 Airfoil, Nonlinear Calculations

Steady state solutions were computed as discussed in Section 2.1 for an NACA 64A006 airfoil for various values of the freestream Mach number by using the ADI scheme with shock fitting outlined in Section 3. The free stream Mach number was varied between 0.8 and 0.9. The mesh system had 101 by 82

grid points in the x- and y-directions respectively. About 250 to 450 time steps were required for the solution to converge $|\Delta\phi|_{max} \leq 10^{-4}$. These steady state solutions are used as initial data for the nonlinear and time-linearized unsteady flow calculations.

Results were computed for the airfoil with quarter-chord flap for various values of the reduced frequency, the free stream Mach number, and the oscillation amplitude, in order to simulate the shock motions observed by Tijdeman (5, 6). These motions were classified by him as: type A - small shock oscillation; type B - the shock becomes very weak or disappears during part of a cycle; type C - the shock leaves the airfoil. Results for type A motions are not given, as they are easy to treat computationally. For all cases studied it took three to six cycles for the flow field to become periodic. Stability seems to require that the time step be small enough that $\Delta t(\text{in degrees})/K < 10$.

Figure 1 illustrates the pressure coefficients on the airfoil surface at various times for $M_\infty = 0.854$, $K = 0.358$ and $\delta = 1°$. For these conditions Ballhaus and Goorjian (12) were able to simulate type B motion where the shock disappears during some part of the cycle. Here the shock does not disappear during the cycle; rather, it becomes quite weak during a small portion of the cycle. This difference is probably due in part to the assumption of a normal shock, which results in a stronger shock than would normally occur, and to the use of shock fitting, which is able to resolve very weak shock waves.

Figure 2 depicts the pressure coefficient on the airfoil surfaces for $M_\infty = 0.822$, $K = 0.496$ and $\delta = 2°$, simulating type C shock motion. Because we have used less spatial resolution and have not scaled the equation and boundary conditions with various powers of the Mach number, a slightly larger

deflection angle seems to be needed in order to generate the type C shock motion; that is, we need a 2° deflection angle rather than the 1.5° of Reference 12 to obtain analogous behavior. In this case the flow field is subcritical during most of the cycle, where the shock wave is barely "captured" in the non-shock-fitting procedure. During the unsteady process the shock moves toward the leading edge. However, the strong singular behavior in pressure at the leading edge prevents the shock from propagating off the airfoil. The perturbation velocity becomes large and is negative; thus, the flow used to calculate the relative velocity ahead of the shock can no longer support a shock wave. Normal shock-fitting calculations determine the shock speed from the pressure jump across the shock at the airfoil surface. This eliminates the possibility that a portion of the shock may propagate off the leading edge in the computations. But this does not imply it cannot occur; rather this is a limitation of the normal shock fitting.

Magnus and Yoshihara (15) have solved the Euler equations using an explicit procedure for the conditions of Figure 1. Their results are compared with our calculation in Figure 3 for two angular times chosen to represent the least and the largest discrepancies. These discrepancies are thought to be mainly due to the inaccuracy of the small perturbation solution near the leading edge. Small errors there change the size and shape of the sonic line and influence the shock's position. For the conditions considered, the shock is nearly normal and the normal shock approximation should be a good one. Rather good agreement is obtained.

Additional nonlinear calculations have been carried out for $M_\infty = 0.880$ and $K = 0.48$. Both pitching and flap motions have been calculated for indicial and harmonic changes. For these conditions very small unsteady changes lead to very small shock motions and the shock wave remains betweed grid

points. Because of the extrapolation procedure used in the shock-fitting, the ξ mesh distribution used here can introduce errors, albeit small ones, in the shock's position when a grid line is crossed. We wished to eliminate these errors in order to use the nonlinear calculations to judge the accuracy of time-linearized calculations. These results indicate that for pitching about mid-chord, nonlinear, amplitude dependent, behavior occurs for $\delta/\tau \geq 0.1$ for $K = 0.48$. Because the amplitude of the shock motions increases with decreasing K, nonlinear effects occur at smaller values of δ/τ at lower reduced frequencies.

Indicial motions require about eight hundred time steps of varying size to resolve the response. For harmonic motions, initiated from rest, three to ten cycles are required for the solution to become harmonic, with large values of K and M_∞ requiring more cycles. The pitching mode requires more cycles than the flap mode. The amplitude of the positive and negative phases of the motion could be varied from cycle to cycle to reduce the number of cycles required. Each cycle requires 60 to 180 time steps to compute, with more steps required for smaller values of K. Each time step takes about 5 seconds of CPU time on a CDC 6400, or about 0.25 seconds of CPU time on a CDC 7600.

4.2 NACA 64A006 Airfoil, Time-Linearized Calculations

Time-linearized results have been computed for an NACA 64A006 airfoil experiencing harmonic and indicial pitching and flap motions. A noted earlier, in the low frequency approximation made here pitching and plunging motions lead to the same result except that the time-linearized perturbations are proportional to the maximum pitch angle for the former, and K times the maximum amplitude for the latter. Harmonic motions initiated from a steady state become nearly periodic in three to ten cycles, with the changes induced

by flap oscillations becoming periodic more rapidly than those resulting from pitching oscillations. More cycles were required for larger reduced frequencies and, to a lesser degree, higher Mach numbers.

In order to confirm the validity of the time-linearized calculations, both the time-linearized and nonlinear algorithms were used to compute the response to a step change in angle of attack and the harmonic response to pitching motions. Figure 4 compares the nonlinear and time-linearized results for the normalized circulation and shock position for harmonic pitching motions at $M_\infty = 0.88$ and $K = 0.48$. Results are given for the fifth cycle; note that the nonlinear results are not yet periodic. Figure 5 compares the nonlinear and time-linearized pressure deviation from steady state at six angular times for the same conditions. Good agreement between the results is obtained for δ/τ less than 0.1.

Time-linearized pressure distributions at six angular positions for an oscillating quarter-chord flap with $K = 0.06$ and $M_\infty = 0.875$ are shown in Figure 6. The flap deflection is downward during the first half of the cycle. The results for the second half of the period, for the symmetrical problem shown here, are just the results shown with the lower and upper surface pressures interchanged. Thus the results for $0°$ are not given as they are just above those for $180°$ with the lower and upper surface pressures reversed. Because the flap hinge occurs very close to the steady state shock location, the pressure singularity due to the change in flow direction at the hinge is missed. The circulation and shock excursion obey the following relations:

$$\Gamma(t)/\delta = 9.26 \sin (t - 59°),$$

$$\chi(t) = 12 \sin (t - 51°).$$

Note the substantial phase lag in the circulation and the shock's position.

Time-linearized pressure distributions at six angular positions for an oscillating airfoil with $K = 0.12$ and $M_\infty = 0.875$ are depicted in Figure 7. If these results are multiplied by K, then they represent the pressure perturbations for a plunging airfoil. As in the previous case of an oscillating flap, changes in forces and moments of $0(\delta/K)$ occur due to shock wave motion. In this case

$$\Gamma(t)/\delta = 5.48 \sin (t - 70°),$$

$$\chi(t) = 5.62 \sin (t - 87°).$$

Analogous computations have been carried out for $K = 0.12$, 0.24, 0.36, and 0.48. Figure 8 depicts the shock wave's exucrsion and maximum circulation as a function of K^{-1}. The nearly linear variation of the shock excursion substantiates an observation made in a one-dimensional model where the shock wave excursion is directly proportional to $1/K$ (see Reference 10).

In these calculations the circulation gives an immediate evaluation of the lift coefficient as a function of time; the moment coefficient must be evaluated by integrating the moment of the pressure coefficient. This is done by integrating the moment of pressure perturbations with the shock wave in its steady-state position and then correcting these results for the moment due to the shock wave motion, assuming that the shock's strength is defined by the steady-state pressure field. This makes an error in the shock strength of $0(\delta)$, but the effect on the moment is $0(\delta^2/K)$; because we have neglected other higher-order terms it is consistent to neglect this change in the strength of the shock wave.

Figure 9 depicts the absolute value and phase angle of the normalized lift and moment coefficients, as a function of the inverse reduced frequency K^{-1}, for harmonic flap and pitching motions at $M_\infty = 0.875$.

The time-linearized algorithm used here is a derivative of that used for the nonlinear calculations. Consequently, computational times are not greatly reduced from those required for the nonlinear calculations. The linearity of these computations may make it possible to greatly reduce the computational effort required. A local stability analysis shows that the computations should be unconditionally stable, but numerical experience has shown some difficulties for $\Delta t(\text{in degrees})/K \geq 50$. Each time step requires about two seconds of CPU time on a CDC 6400, or about 0.1 seconds on a CDC 7600. The number of time steps required for a given computation is somewhat less than those required for the nonlinear computations at small values of K, and comparable at larger values of K.

5. CONCLUSION

Efficient and accurate methods for computing low frequency, unsteady behavior in transonic flows have been developed. They utilize the ADI procedure developed at NASA Ames for the small perturbation equation, but treat shock waves as discontinuities. The time-linearized calculations allow shock wave motions, which are shown to be $O(\delta/K)$ and often dominate changes in the force and moment coefficients. Comparison of the time-linearized results with fully nonlinear calculations delineates their range of applicability. The unsteady behavior due to harmonic pitching and flap oscillations of an NACA 64A006 airfoil is discussed.

REFERENCES

1. Ballhaus, W. F.: Some Recent Progress in Transonic Flow Computations. VKI Lecture Series on Computational Fluid Dynamics, von Karman Institute for Fluid Dynamics, Rhode-St-Genese, Belgium, 1976.

2. Landahl, M. T.: Unsteady Transonic Flow. Pergamon Press, New York, 1961, 111-113.

3. MacCormack, R. W.: An Efficient Numerical Method for Solving the Time-Dependent Navier-Stokes Equations at High Reynolds Number. NASA TM X-73129, 1976.

4. Levy, L. L., Jr.: An Experimental and Computational Investigation of the Steady and Unsteady Transonic Flow Field About an Airfoil in a Solid-Wall Test Channel. AIAA Paper No. 77-678, 1977.

5. Tijdeman, H.: On the Motion of Shock Waves on an Airfoil with Oscillation Flap in Two-Dimensional Transonic Flow. NLR TR 75038U, 1975.

6. Tijdeman, H.: On the Motion of Shock Waves on an Airfoil with Oscillating Flap. Ed. K. Oswatitsch and D. Rues, IUTAM Symposium Transsonicum II, Göttingen, 1975, 49-56.

7. Tijdeman, H., Schippers, P., and Persoon, A. J.: Unsteady Air Loads on an Oscillating Supercritical Airfoil. NLR MP 77008 U, 1977.

8. Traci, R. M., Albano, E., and Farr, J. L.: Perturbation Method for Transonic Flows about Oscillating Airfoils. AIAA J., Vol. 14, No. 9, 1976, 1258-1265.

9. Weatherill, W. H., Ehlers, R. E., and Sebastian, J. D.: Computation of the Transonic Perturbation Flow Fields Around Two- and Three-Dimensional Oscillating Wings. NASA CR-2599, 1975.

10. Fung, K-Y., Yu, N. J., and Seebass, A. R.: Small Unsteady Perturbations in Transonic Flows. Informal report, submitted for publication 1977.

11. Ballhaus, W. F. and Steger, J. L.: Implicit Approximate-Factorization Schemes for the Low-Frequency Transonic Equation. NASA TM X-73082, 1975.

12. Ballhaus, W. F. and Goorjian, P. M.: Implicit Finite Difference Computations of Unsteady Transonic Flows about Airfoils, Including the Treatment of Irregular Shock Wave Motions. AIAA Paper 77-205, 1977.

13. Ballhaus, W. F. and Lomax, H.: The Numerical Simulation of Low Frequency Unsteady Transonic Flow Fields. Lecture Notes in Physics, Springer-Verlag, Vol. 35, 1975, 57-63.

14. Magnus, R. and Yoshihara, H.: Unsteady Transonic Flows Over an Airfoil. AIAA J., Vol. 13, No. 12, 1975, 1622-1628.

15. Magnus, R. and Yoshihara, H.: The Transonic Oscillating Flap. AIAA Paper No. 76-327, 1976.

16. Magnus, R. J.: Computational Research on Inviscid, Unsteady, Transonic Flow over Airfoils. ONR Report CASD/LVP 77-010, 1977.

17. Caradonna, F. X. and Isom, M. P.: Numerical Calculation of Unsteady Transonic Potential Flow Over Helicopter Rotor Blades. AIAA J., Vol. 14, No. 4, 1976, 482-488.

18. Beam, R. M. and Warming, R. F.: An Implicit Finite-Difference Algorithm for Hyperbolic Systems in Conservation-Law Form. Journal of Computational Physics, Vol. 22, No. 1, 1976, 87-110.

19. Ballhaus, W. F., Jameson, A., and Albert, J.: Implicit Approximate Factorization Schemes for the Efficient Solution of Steady Transonic Flow Problems. AIAA 3rd Computational Fluid Dynamics Conference, June, 1977, 27-34.

20. Yu, N. J. and Seebass, A. R.: Inviscid Transonic Flow Computations with Shock Fitting. Ed. K. Oswatitsch and D. Rues, IUTAM Symposium Transsonicum II, Göttingen, 1975, 449-456.

21. Yu, N. J., Seebass, A. R., and Ballhaus, W. F.: An Implicit Shock-Fitting Scheme for Unsteady Transonic Flow Computations. AIAA 3rd Computational Fluid Dynamics Conference, June, 1977, 13-26.

22. Ballhaus, W. F. and Goorjian, P. M.: Computation of Unsteady Transonic Flows by the Indicial Method. AIAA Paper No. 77-477, 1977.

23. Traci, R. M., Albano, E. D., and Farr, J. L., Jr.: Perturbation Method for Transonic Flow about Oscillating Airfoils. AIAA Paper No. 75-877, 1975.

24. Traci, R. M., Albano, E. D., Farr, J. L., Jr., and Cheng, H. K.: Small Disturbance Transonic Flows about Oscillating-Airfoils. Air Force Flight Dynamics Laboratory, Wright-Patterson Air Force Base, Ohio, AFFDL-TR-75-100, 1974.

25. Ehlers, F. E.: A Finite Difference Method for the Solution of the Transonic Flow About Harmonically Oscillating Wings. NASA CR-2257, 1974.

26. Krupp, J. A. and Cole, J. D.: Studies in Transonic Flow IV, Unsteady Transonic Flow. UCLA Engineering Report 76104, 1976.

27. Lin, C. C., Reissner, E., and Tsien, H. S.: On Two-Dimensional Non-Steady Motion of a Slender Body in a Compressible Fluid. J. Math. and Physics, 27, 1948, 220-231.

28. Hafez, M. M. and Cheng, H. K.: Shock-Fitting Applied to Relaxation Solutions of Transonic Small-Disturbance Equations, AIAA J., Vol. 15, No. 6, 1977, 786-793.

29. Murman, E. M.: Analysis of Embedded Shock Waves Calculated by Relaxation Methods. AIAA J., Vol. 12, No. 5, 1973, 626-633.

30. Moretti, G.; Thoughts and Afterthoughts about Shock Computations. PIBAL Report No. 72-37, 1972.

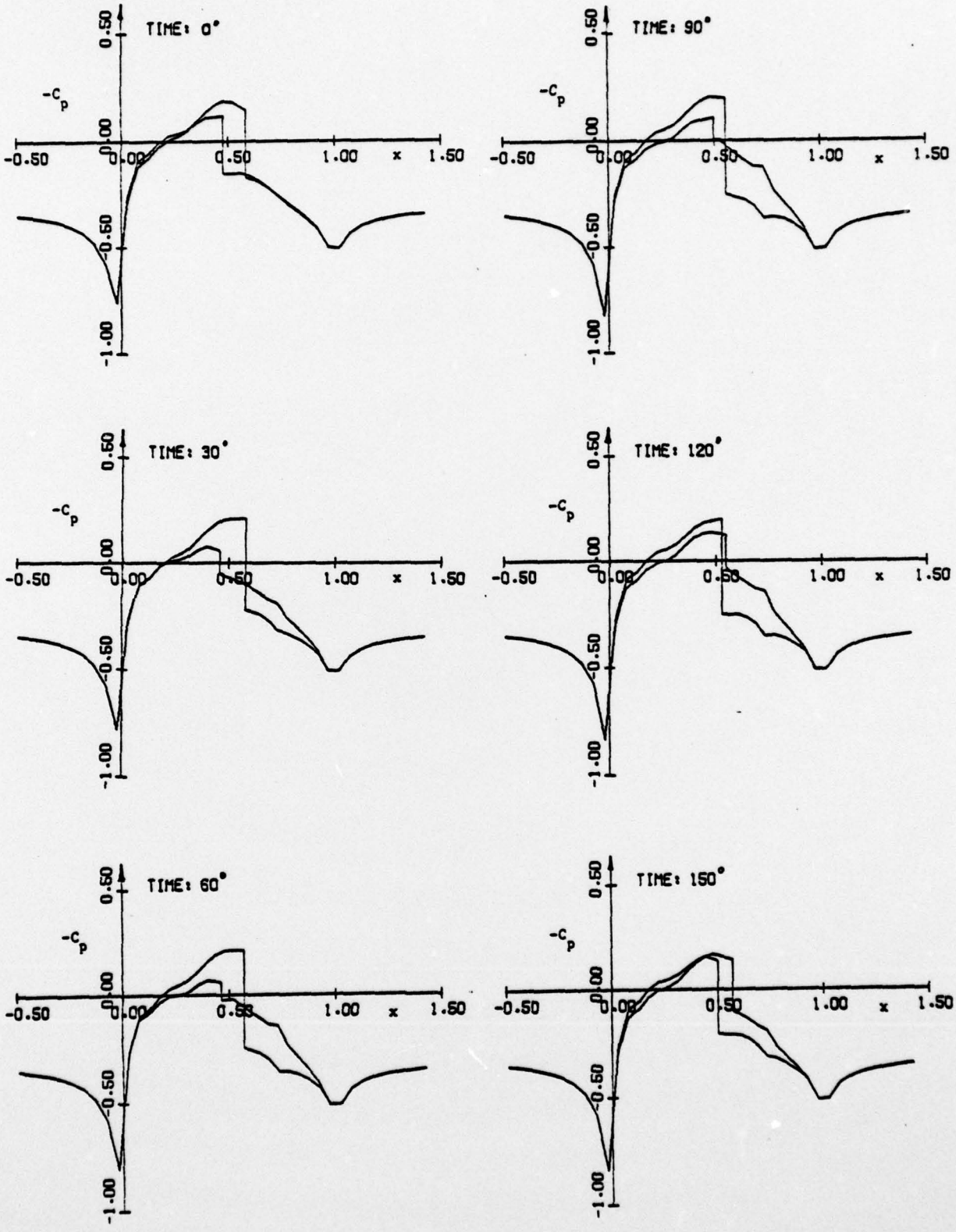

FIGURE 1. C_p ON AN NACA 64A006 AIRFOIL AT $M_\infty = 0.854$, $K = 0.358$ WITH $\delta = 1° \sin t$ (NONLINEAR CALCULATIONS).

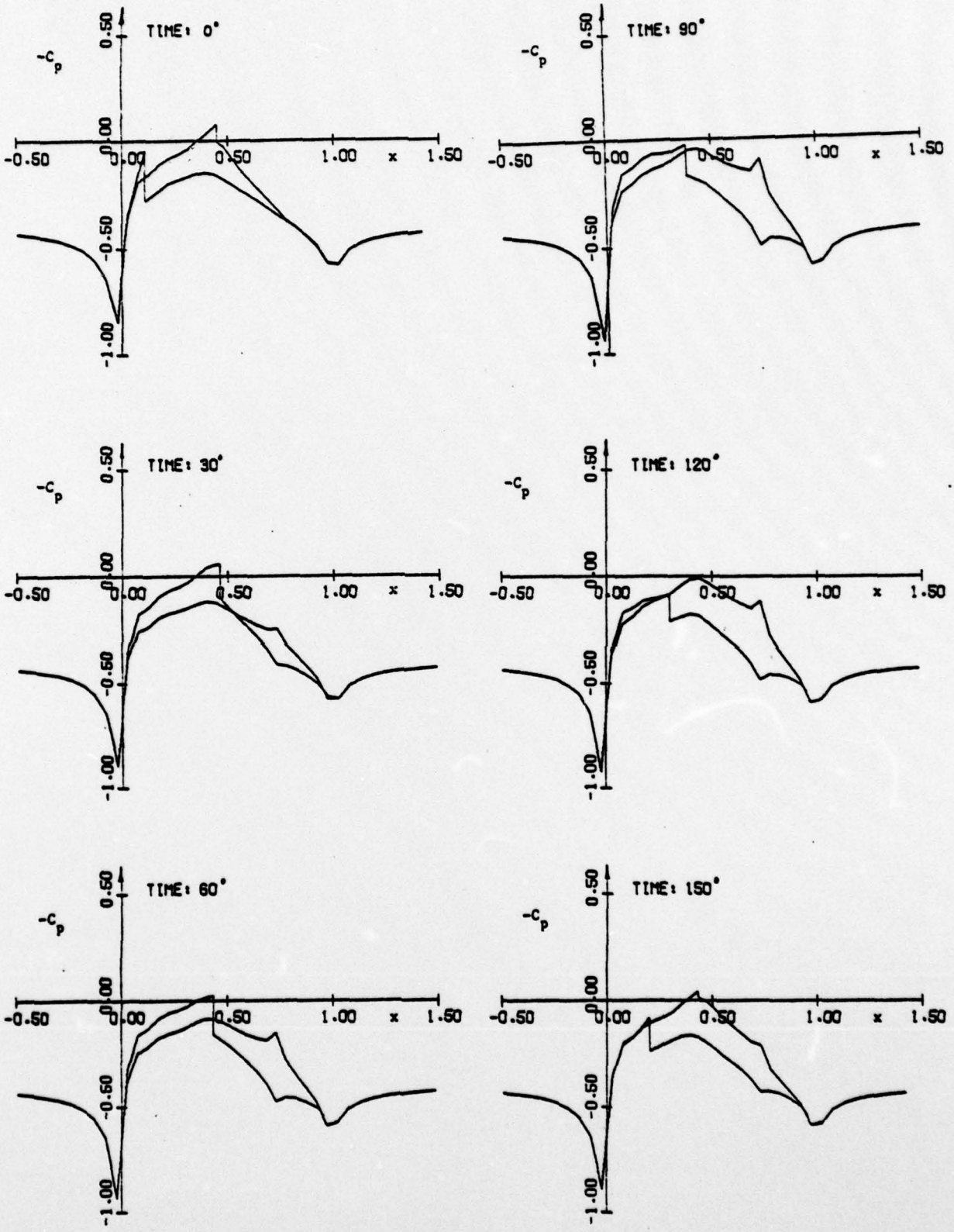

FIGURE 2. C_p ALONG AN NACA 64A006 AIRFOIL AT $M_\infty = 0.822$, $K = 0.496$ WITH $\delta = 2° \sin t$ (NONLINEAR CALCULATIONS).

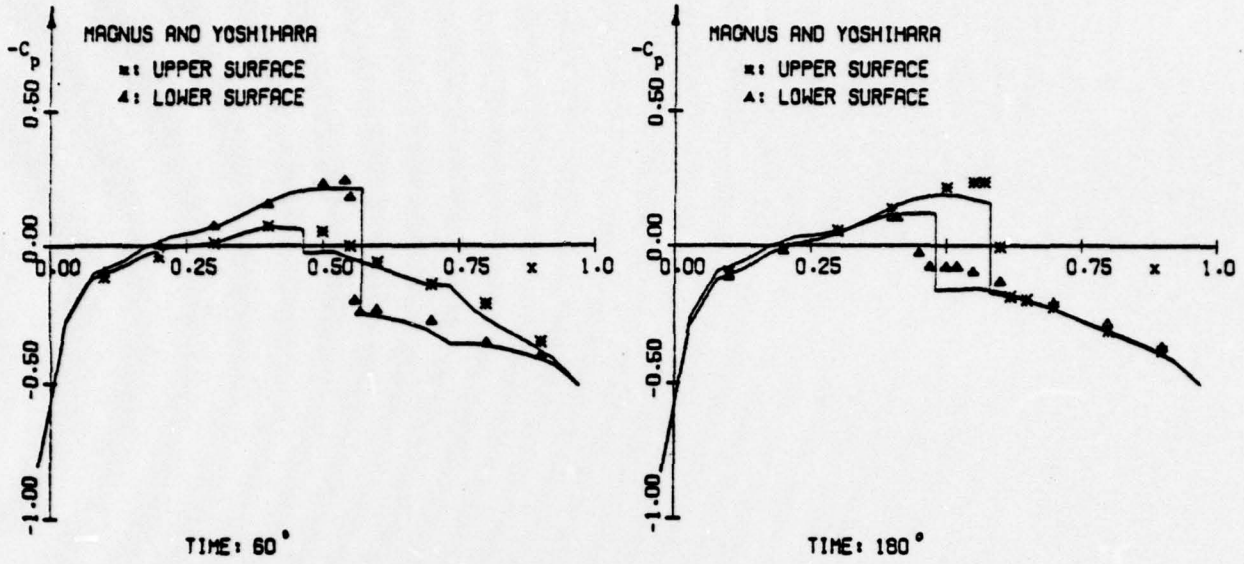

FIGURE 3. COMPARISONS OF THE RESULTS FOR C_p ON AN NACA 64A006 AIRFOIL, AT $M_\infty = 0.854$, $K = 0.358$ WITH $\delta = 1°$ sin t, WITH THOSE OF MAGNUS AND YOSHIHARA (NONLINEAR CALCULATIONS).

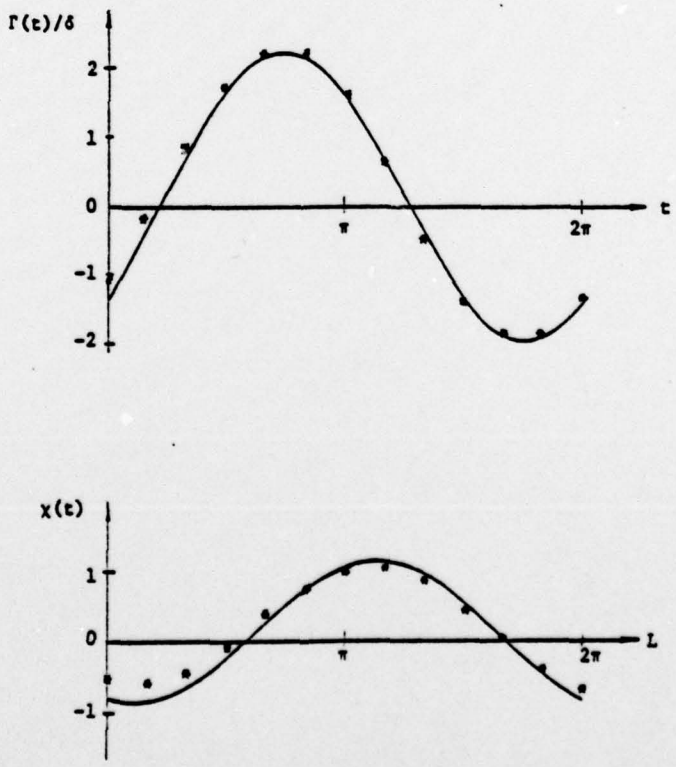

FIGURE 4. NONLINEAR (***) AND TIME-LINEARIZED(——) CIRCULATION AND SHOCK POSITION FOR THE PITCHING MOTION OF AN NACA 64A006 AIRFOIL. RESULTS SHOWN ARE FOR THE FIFTH CYCLE. THE NONLINEAR RESULTS ARE FOR $\delta = 0.1°$ AND ARE NOT YET PERIODIC. $M_\infty = 0.880$, $K = 0.48$.

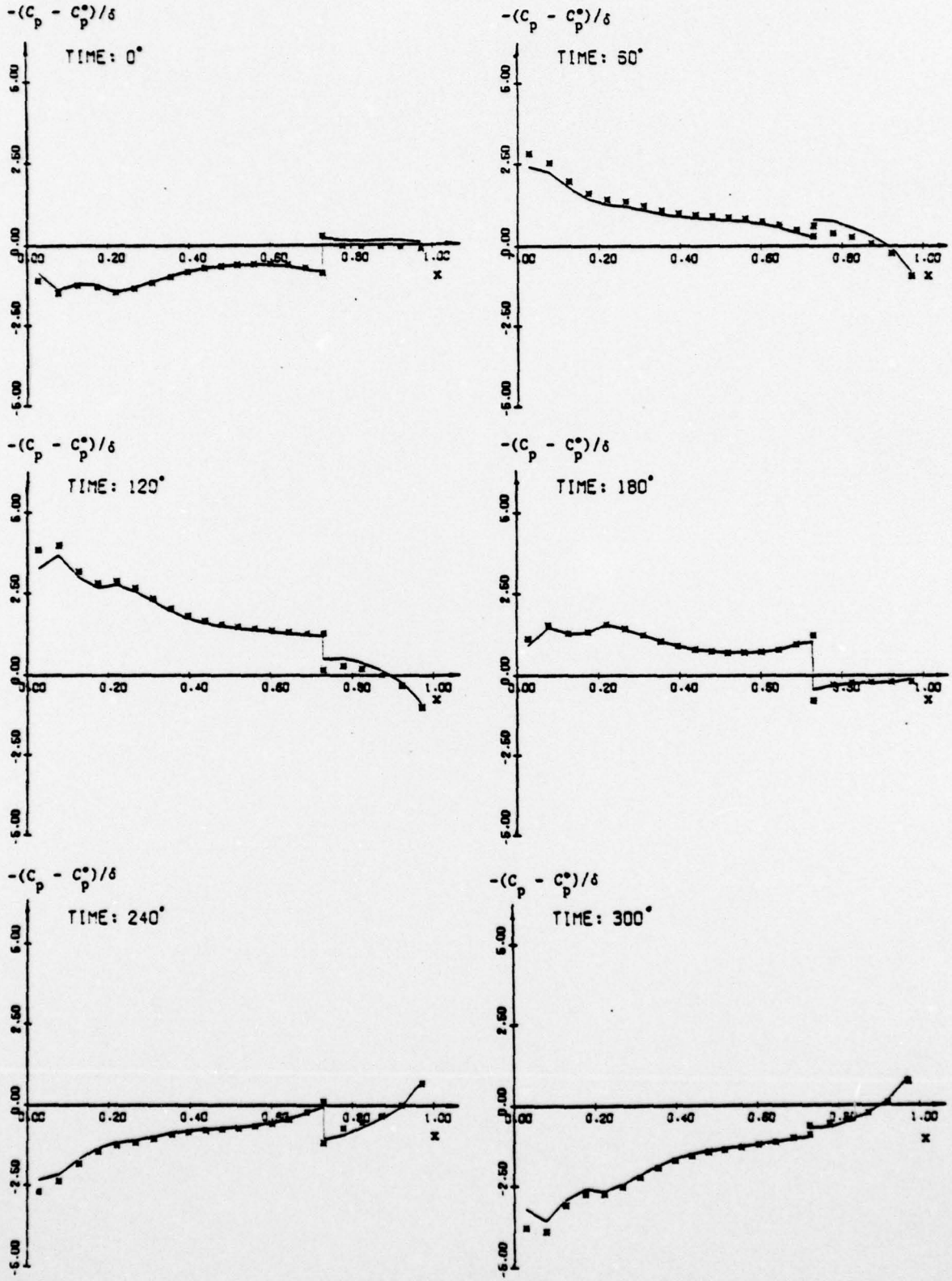

FIGURE 5. NORMALIZED NONLINEAR (****) AND TIME-LINEARIZED (——) PRESSURE PERTURBATIONS ON THE UPPER SURFACE OF AN NACA 64A006 AT SIX TIMES. PITCHING MOTION WITH $M_\infty = 0.880$, $K = 0.48$. FOR THE NONLINEAR CALCULATIONS $\delta = 0.1°$.

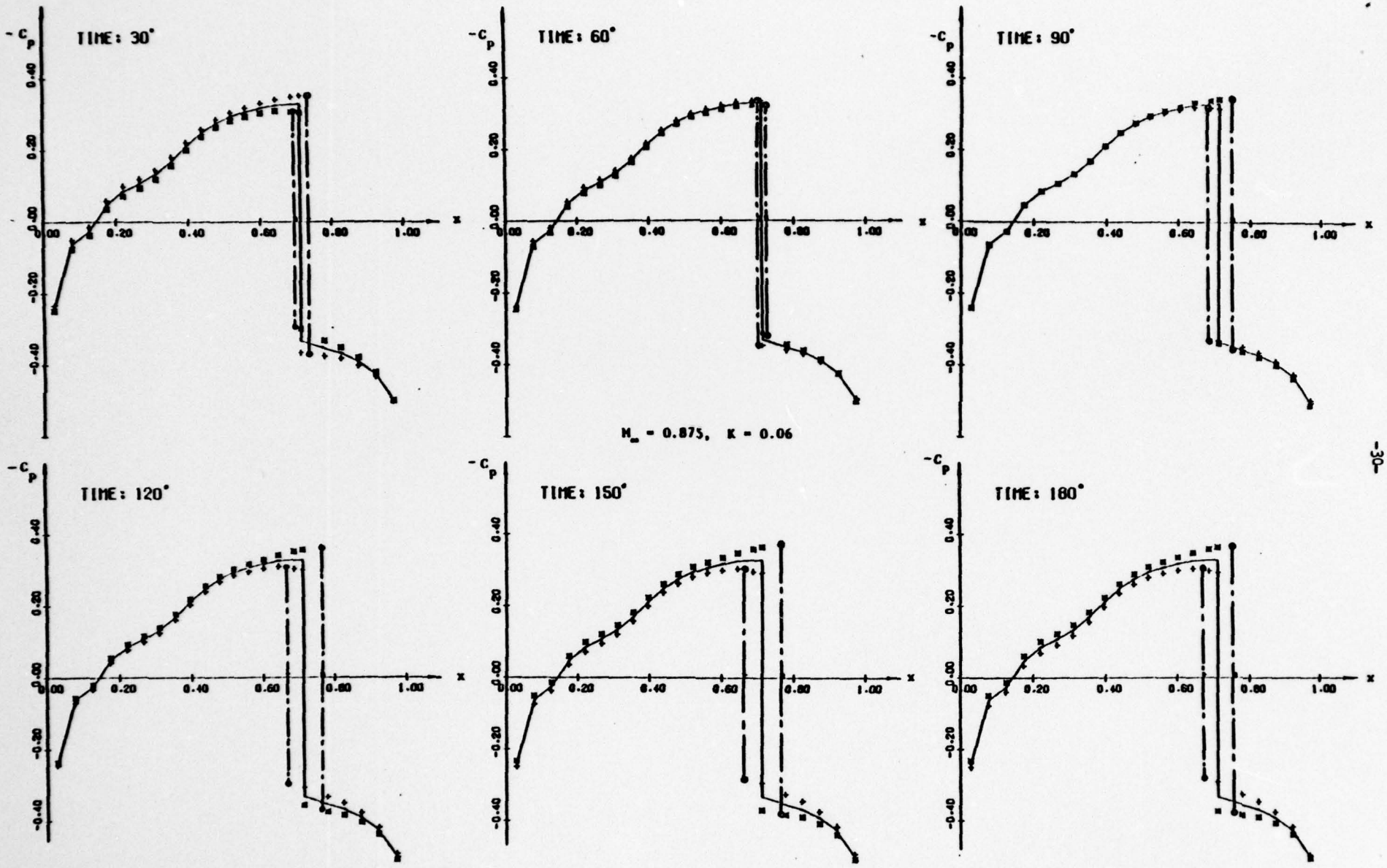

FIGURE 6. TIME-LINEARIZED PRESSURE COEFFICIENTS ON THE UPPER (+) AND LOWER (*) SURFACES OF AN NACA 64A006 AIRFOIL WITH OSCILLATING QUARTER-CHORD FLAP ($\delta = 1/4°$).

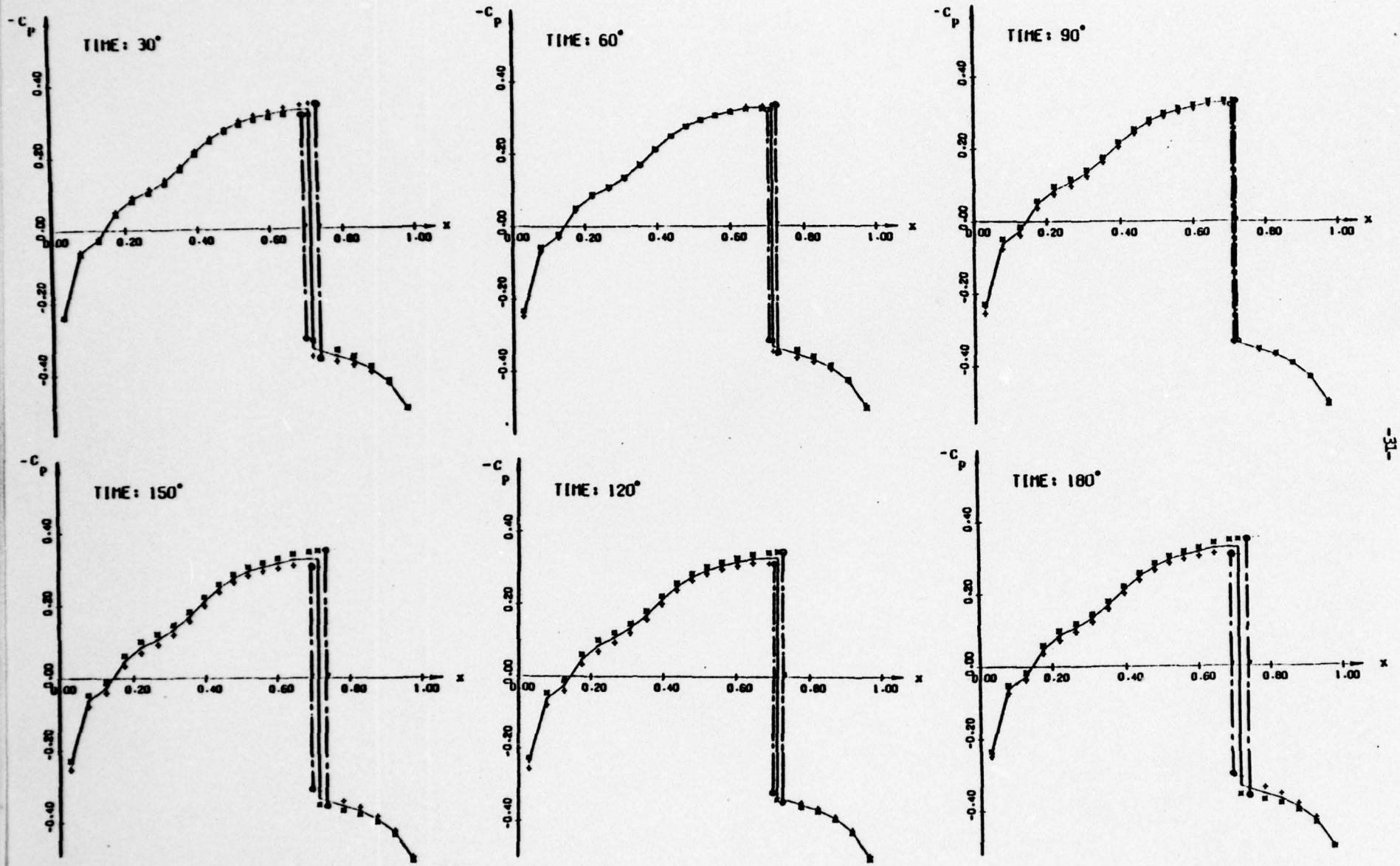

FIGURE 7. TIME-LINEARIZED PRESSURE COEFFICIENTS ON THE UPPER (+) AND LOWER SURFACES OF AN NACA 64A006 AIRFOIL OSCILLATING IN PITCH (δ = 1/4°). M_∞ = 0.875, K = 0.12.

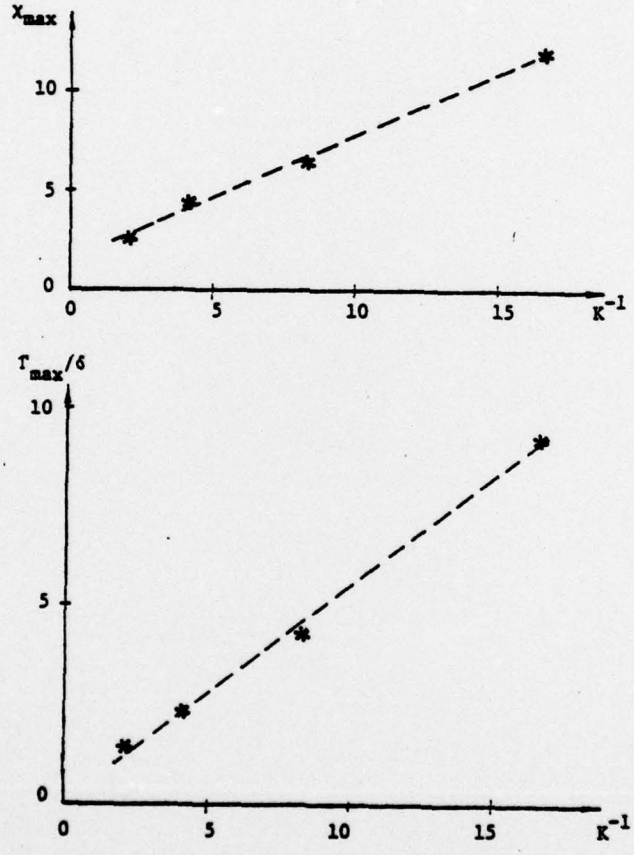

FIGURE 8. NORMALIZED MAXIMUM SHOCK EXCURSION AND CIRCULATION AS A FUNCTION OF INVERSE REDUCED FREQUENCY FOR AN NACA 64A006 AIRFOIL WITH OSCILLATING QUARTER-CHORD FLAP. $M_\infty = 0.875$.

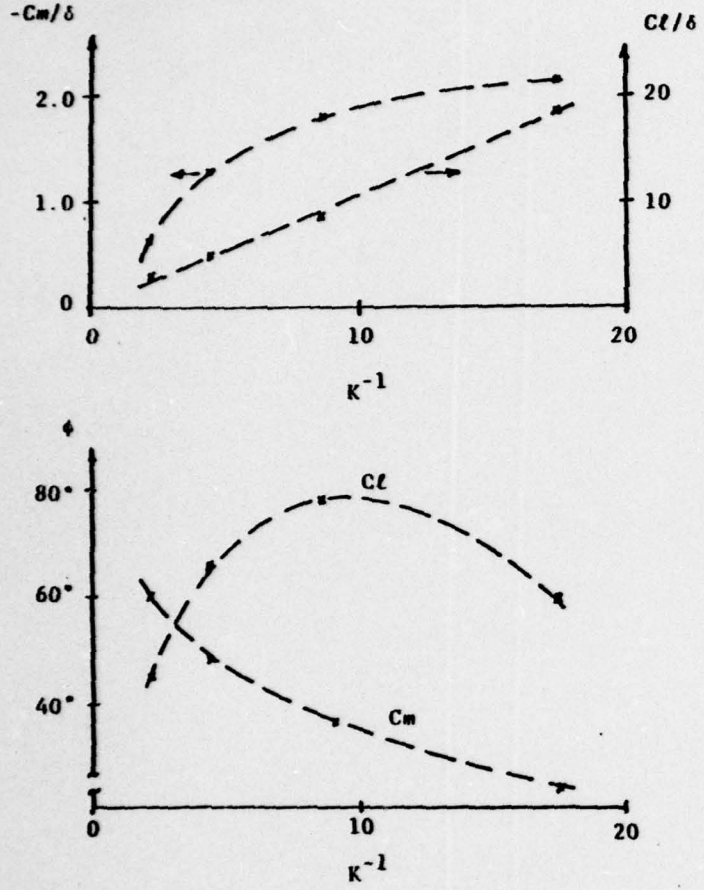

NORMALIZED LIFT AND MID-CHORD MOMENT COEFFICIENT AMPLITUDES AND PHASE LAGS FOR AN NACA 64A006 AIRFOIL WITH HARMONIC FLAP OSCILLATIONS AT $M_\infty = 0.875$.

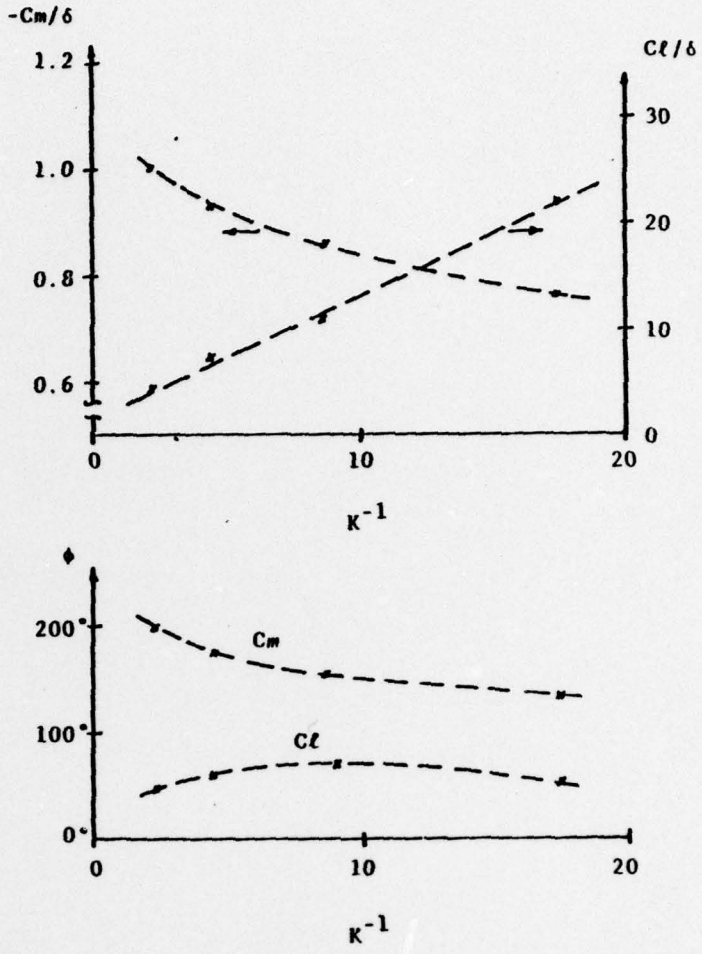

NORMALIZED LIFT AND MID-CHORD MOMENT COEFFICIENT AMPLITUDES AND PHASE LAGS FOR HARMONIC PITCHING MOTIONS OF AN NACA 64A006 AIRFOIL AT $M_\infty = 0.875$.

FIGURE 9.